Journal of Power Sources 261 (2014) 162–169

Contents lists available at ScienceDirect

Journal of Power Sources

journal homepage: www.elsevier.com/locate/jpowsour

Short communication

Evaluation of corrosion resistance of aluminium coating with and without annealing against molten carbonate using electrochemical impedance spectroscopy

C.S. Ni [1], L.Y. Lu [1], C.L. Zeng, Y. Niu*

State Key Laboratory for Corrosion and Protection, Institute of Metal Research, Chinese Academy of Sciences, Shenyang 110016, PR China

HIGHLIGHTS

- Arc ion plating was used to fabricate pure Al coating on 310S stainless steel.
- EIS is employed to evaluate the impact of high-temperature annealing on the Al coating.
- Two distinct sets of impedance spectra are obtained for the aluminide from with/without high-temperature annealing.
- Microstructure tends to have great impact on the corrosion mechanism of the Al–Fe coating.

ARTICLE INFO

Article history:
Received 25 November 2013
Received in revised form
5 March 2014
Accepted 18 March 2014
Available online 27 March 2014

Keywords:
Stainless steel
Molten salts
Intermetallics
Electrochemical impedance spectroscopy
Hot corrosion

ABSTRACT

An arc ion plating (AIP) was used to fabricate a FeAl layer on 310S stainless steel to protect the sealing area being corroded by the molten carbonate in molten carbonate fuel cells (MCFCs). The degradation of aluminide coatings comes from both the corrosion of the coating in contact with the molten carbonate and the aluminium depletion due to the interdiffusion of aluminium and the substrate. The in-situ forming of aluminide in molten carbonate at 650 °C could be a possible way to reduce the inward diffusion of aluminium in the conventional pre-annealing at 850 °C. Electrochemical impedance spectroscopy (EIS) measurements were performed to model the corrosion of this pre-formed FeAl coating in comparison with the one formed in-situ in molten (0.62 Li+0.38 K)$_2CO_3$ at 650 °C. Although α-$LiAlO_2$ is the corrosion product in both cases, the impedance spectra show distinct rate-limiting steps; the former is controlled by the charged particles passing through the scale, while the latter by their diffusion in the melt. The microstructure of the scale might be the reason for the difference in corrosion mechanism.

1. Introduction

The molten carbonates at 650 °C cause significant corrosion problems to the construction materials of Molten Carbonate Fuel Cells (MCFC) [1–4] and the aluminide alloys and coatings are recommended to reduce the corrosion in the wet-sealing area, where, unlike the current-collection area, the materials require no conductivity [5,6]. Aluminide will react with molten carbonates to form a thin layer of corrosion-resistant $LiAlO_2$ which, if porous, is also the matrix material for the electrolyte of MCFC to retain molten carbonates.

The corrosion of Fe–Al alloys in molten carbonates has been studied using weight-gain and electrochemical methods [7–10]. Acidic fluxing of yttria in the Oxide-Dispersion-Strengthened (ODS) FaAl alloy was accused of the pitting corrosion because of the active-passive electrochemical cells between the interior of pits and the external surface [7]. The impedance spectra of Fe − 40 at. % Al − 0.5 at. % B were reported to consist of two capacitance arcs after 20-h immersion in molten (0.62 Li + 0.38 K)$_2CO_3$ at 650 °C, and the corrosion of Fe–Al was controlled by the diffusion of charged particles through the scale from then on [8]. In addition, Jun [9] reported that the FeAl alloy required a minimum of 25 at. % Al to form a continuous $LiAlO_2$ scale in Li/K carbonate melt at 650 °C, and the microstructure features of the scale and the alloy surface had a great influence on the corrosion behaviour.

Because stainless steels, particularly austenitic steels, are the construction material of MCFC and aluminide alloy shows poor mechanical properties, so the application of aluminide coatings on

* Corresponding author. Tel.: +86 23971375; fax: +86 2397 3086.
E-mail address: yniu@imr.ac.cn (Y. Niu).
[1] Present address: School of Chemistry, University of St Andrews, Fife KY16 9ST, Scotland.

http://dx.doi.org/10.1016/j.jpowsour.2014.03.076
0378-7753/

stainless steel has more practical significance. The pure aluminium coatings can be fabricated using low-cost spraying or slurry technique, and they will interact with the stainless-steel substrate to form an aluminide coating in the subsequent annealing process at a temperature above 800 °C [11–14]. Aguero et al. [11] and Perez et al. [12] used EIS to study the corrosion of the coatings from the thermal spray and the slurry technique in molten carbonates respectively; two capacitance arcs could be distinguished from the Nyquist plots and the polarisation resistance was used to estimate the corrosion rate. Furthermore, Frangini et al. [15,16] reported the results obtained by depositing a layer of FeAl intermetallic alloy directly onto 316L austenitic stainless steel using the Electrospark Deposition (ESD) technique to circumvent the annealing process, and found that after 1000-h immersion test, the aluminide coating suffered from degradation owing to the microcrack and Al-depletion.

Because the annealing process would add to the cost of the coating process, a high-quality aluminide coating could be formed at the start-up stage of the MCFC if a pure aluminium coating was applied [17]. The omission of pre-annealing process could reduce the processing cost and the aluminium loss in the protective layer because of the interdiffusion between the aluminium and the substrate at high temperature. However, no corrosion behaviour of this method has been reported and the corrosion mechanism of fresh aluminium coating in molten carbonate is not very clear. This paper serves to study the corrosion-resistant property of the pure Al coating immersed directly into molten carbonates at 650 °C in comparison with the pre-formed Al–Fe coating at 850 °C. Interestingly, the immersion of the pure Al coating into the molten carbonates produces a layer of FeAl aluminide after 120 h immersion, but its corrosion behaviour is distinct from that of pre-formed FeAl coating.

In studying the corrosion of aluminide coatings against molten carbonates, the state-of-the-art ion plating Al coating [12,15,18] which is known to provide a dense and coherent coating. The AIP is employed in this study to produce an adherent and compact coating for studying the effect of high-temperature annealing on the corrosion mechanism in molten carbonate by eliminating the factors like microcrack, voids and compositional segregation and complex phases that would complicate the explanation. The universally-claimed lithiation process at the beginning of the corrosion process can be inferred from the electrochemical impedance data very easily for the first time. In addition, the high quality coating is also beneficial to illustrate the typical impedance models for the corrosion of coatings in molten salt.

2. Experimental

2.1. Materials preparation

The commercial 310S stainless steel (Fe – 26.37 wt. % Cr – 18.5 wt. % Ni – 1.4 wt. % Mn with a trace amount of $P < 0.45$ wt. %, $S < 0.03$ wt. % and $C < 0.08$, wt. %) was cut into 16 × 8 × 2 mm with a hole of 1.5 mm in diameter, ground to 800 grit sand paper and cleaned in acetone using ultrasonic bath before the deposition of Al coating. The cathode target of AIP in this work is pure Al (99.99 wt. %). The deposition chamber was evacuated to the pressure of 8×10^{-3} Pa and the chamber was heated simultaneously to 120 °C to remove the residual gas adsorbed on the chamber wall and samples. Then the Al target was initiated at the bias voltage of 800 V for 3 min to sputter clean the surface of the substrate. After that, the deposition was carried out to deposit an Al coating of ~10 μm, and the parameters are listed in Table 1, similar to those in reference [19].

After being sealed in an evacuated quartz tube containing slight argon gas, several of the samples were annealed at 850 °C for 200 min and called as-annealed samples. Two of the as-annealed samples or the as-deposited samples, after an Fe – 25 wt. % Cr – 1 wt. % Al lead wire being attached to each sample at the end of Φ 1.5 mm hole, were sealed in alumina tubes with high-temperature cement to form a two-electrode system. The surface area of each working electrode was 0.8 cm^2. The two-electrode system was used to avoid the potential change of the reference electrode in a three-electrode system for long-term EIS tests. The setup of the experiment is illustrated in Fig. 1 [14,20].

Table 1
Parameters for the multi-arc ion plating used for Al deposition.

Working pressure (Pa)	$5–8 \times 10^{-3}$
Arc voltage (V)	20–24
Arc current (A)	60–65
Bias voltage (V)	−220
Bias duty cycle (%)	33.00
Temperature (°C)	200–300
The distance between targets and substrates (mm)	120.00

2.2. Electrochemical test and characterization

The mixed powder of 62% Li_2CO_3 + 38% K_2CO_3 (in mole ratio) was put in a furnace, then heated up to 350 °C and stabilised for 24 h to purge the trace amount of moisture. The furnace was kept at 650 °C during the electrochemical tests. The electrode was put into the melt at 650 °C afterwards and EIS data were retrieved at fixed intervals. The electrochemical impedance measurements were carried out in the frequency range of 10^5–10^{-2} Hz using a computer-controlling M398 Impedance Test System containing a Potentiostat 263A of Princeton Applied Research (PAR) and an M5210 lock-in amplifier. The amplitude of input sine signal was 10 mV. A Fourier transform technique was employed for frequencies in the range of 0.01–1.13 Hz to increase measurement speed and lower the degree of perturbation to the cell. The impedance spectra were calculated and fitted with Zview software.

The coatings before and after the electrochemical tests were also characterised by X-ray diffraction (XRD) and scanning electron

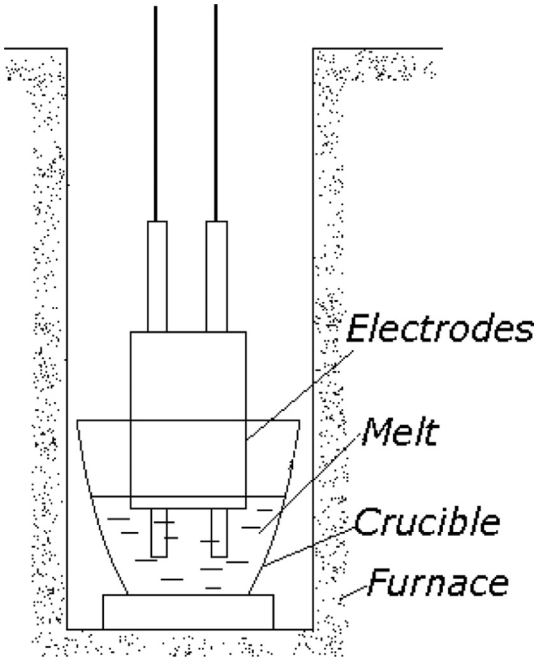

Fig. 1. Set-up of the electrochemical tests and the assembly of two-electrode system.

microscopy (SEM) equipped with energy dispersive X-ray analysis (EDX).

3. Results and discussion

3.1. Morphology of the Al coating before and after high-temperature annealing

The cross-sectional images of the as-deposited and as-annealed coatings are shown in Fig. 2. The EDX line scan in Fig. 2(c) and (d) shows the spatial distribution of aluminium on the surface of alloys. In Fig. 2(a), a coherent interdiffusion layer (average composition: Al – 5.41 at. % Fe – 3.31 at. % Cr – 1.95 at. % Ni – 0.4 at. % Mn by EDX) of 3.5-μm thickness on the substrate is covered by a continuous but wavy Al layer. On the contrary, an evenly distributed aluminide coating covers the surface after the high-temperature annealing process as shown in Fig. 2(b). The EDX composition of the FeAl layer in the as-annealed coating is Fe – 49.61 at. % Al – 13.17 at. % Cr – 6.72 at. % Ni on the surface layer and the XRD curve verifies the phase of FeAl. An interdiffusion zone where the Cr or Ni enriches (Fig. 2(d)) can be identified in between the FeAl layer and the substrate. For an Fe–Al diffusion couple, the Fe and Al tracer diffusivity at the low Al side in the A2-disordered state are four-order magnitude as larger as that at the high Al side in the B2-ordered state [21], so the formation of B2-ordered FeAl phase is attributed to Fe diffusion at the low Al side before the formation of final FeAl phase. The surface morphologies of the coatings before and after the annealing process, as shown in Fig. 3(a) and (b), respectively, are very different; the surface of the as-deposited Al coating develops a loose surface containing flakes and beads of 2–5 μm, while the as-annealed sample shows relatively uniform curves with dimensions between 1 and 2 μm.

3.2. Phase and morphology analysis of the corrosion product

Fig. 4 shows the XRD results of the as-annealed and as-deposited coating after the 120-h corrosion. The original Al coating transforms to a layer of FeAl intermetallics during the corrosion as can be indicated in Fig. 4(a). The scales formed on both coatings are α-$LiAlO_2$ according to XRD curves. The relative intensity of α-$LiAlO_2$ peaks of Al–Fe in Fig. 4(a) is stronger than that in Fig. 4(b), indicating a thicker layer of corrosion products on the as-deposited Al sample. According to Vossen et al. [22], α-$LiAlO_2$ was also the protective product of Ni-50 at. % Al intermetallics against the corrosion of molten carbonates. At 650 °C, α-$LiAlO_2$ in molten carbonates was stable even after 33 000 h without converting into γ-$LiAlO_2$ and showed a good durability [23].

Even though an Al–Fe coating containing Fe – 40.2 at. % Al – 16 4 at. % Cr – 5.1 at. % Ni (EDX composition) has been retained on the surface of as-deposited sample after 120 h annealing in the molten

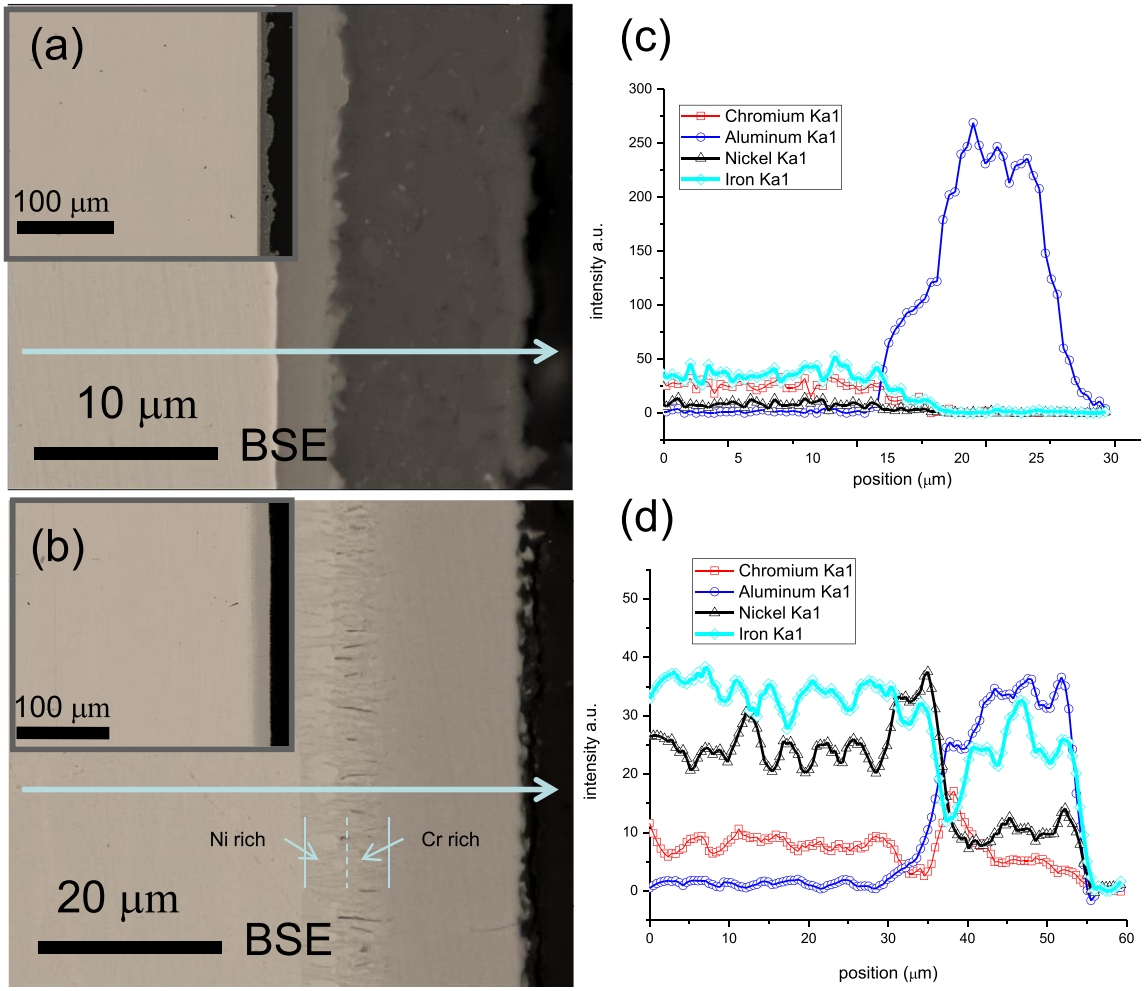

Fig. 2. SEM of the as-deposited coating (a) and as-annealed coating (b); the inserts are the low-magnification images. (c) and (d) are the EDX line scans in image (a) and (b), respectively. The regions of Ni- or Cr-rich area are indicated in image (b).

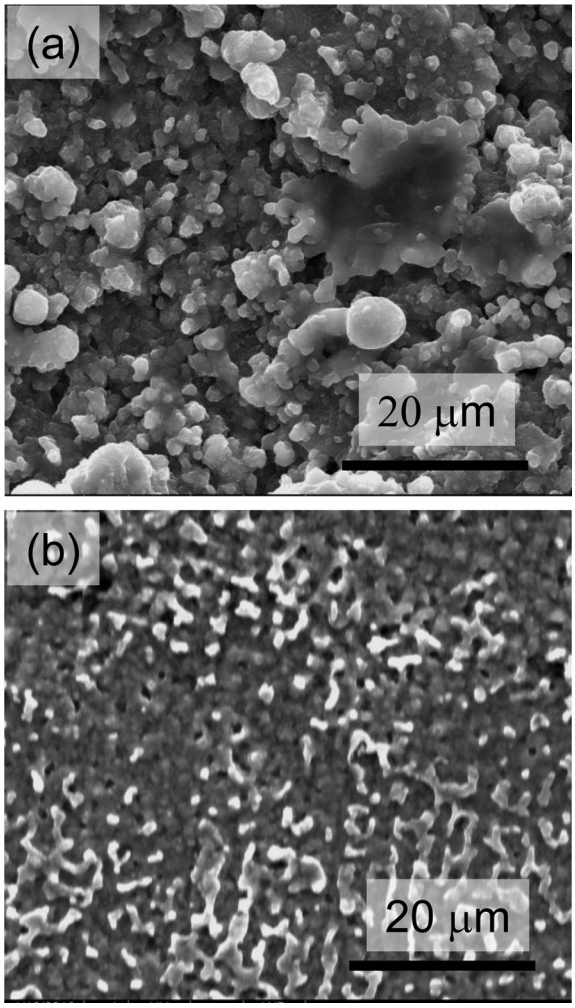

Fig. 3. Surface morphology of the as-deposited coating (a) and as-annealed coating (b).

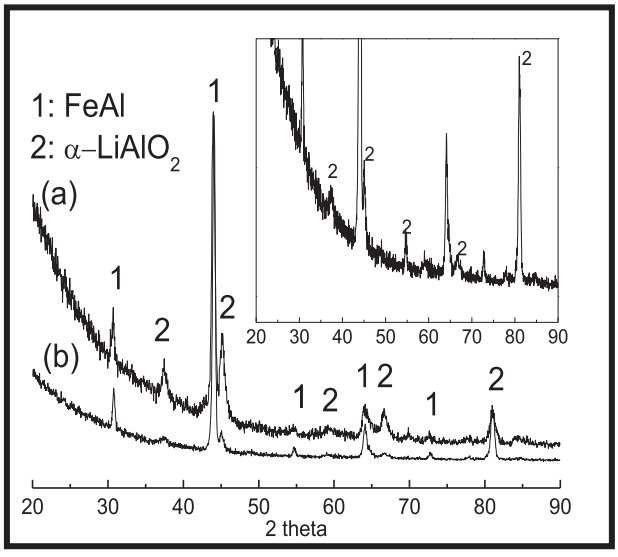

Fig. 4. XRD pattern of as-deposited coating (a) and as-annealed coating (b) after 120 h immersion in molten carbonate at 650 °C. The insert is used to magnify the peaks of α-$LiAlO_2$ of as-annealed sample in (b).

carbonates, its scale morphology and thickness is significantly different from that of the as-annealed samples. The cross-sectional images of the corroded samples are shown in Fig. 5. The bright particles are Cr-rich precipitates (Fe – 34.1 at. % Al – 34.3 at. % Cr – 2.1 at. % Ni by EDX) in aluminide layer and can be attributed to the diffusion of Cr from the substrate. When the Al coating on 3l0S stainless steel was annealed at 650 °C without molten carbonate, Cr-rich particles were also found in reference 13.

The aluminide layer of the as-annealed sample after the 120-h immersion test in molten carbonate at 650 °C in Fig. 5(b) is thicker than that of the initial state in Fig. 2(b). The composition of the aluminide layer by EDX is Fe – 33.3 at. %Al – 16.7 at. %Cr – 8.3 at. % Ni; i.e., the Al composition) is decrease from around 50 at. % to around 33 at.%, because of the interdiffusion between Al and the surface to the substrate after the formation of FeAl phase [24]. A comparison of the composition between the two coatings after 120 h annealing in molten carbonate shows that the sample without pre-annealing is 7 at.% higher, while the compositions of nickel and chromium are similar. An ultra thin layer of corrosion product is found on the as-annealed sample, Fig. 5(b), but an indented oxide layer outgrows on the FeAl layer of the as-deposited sample, as indicated in Fig. 5(a), where some bright particles can also be found in the FeAl layer.

3.3. EIS for the Al coatings with and without high-temperature annealing

Fig. 6(a) is the impedance spectra of the as-deposited Al coating in molten carbonate at different times. The impedance spectra contain a well-formed loop at high frequency and a straight line at low frequency. The modulus of impedance increases rapidly from 2 h to 12 h and levels off afterwards. The low modulus of impedance at 2 h can be partially attributed to the large area of the rough surface as shown in Fig. 3.

The impedance spectra of the annealed sample show two loops, a large one at the low-frequency part and a small one at the high-frequency part. Two loops can be inferred easily from the Bode plots, and the small loops are magnified by the inserts in Fig. 6(b). The modulus of the impedance starts from a large value of 500 Ω cm [2] at 2 h, decreases to250 Ω cm [2] in the first 12 h and then stabilises at 450 Ω cm [2] after 72 h.

3.4. Interpretation of impedance spectra

The electrochemical process of hot corrosion can be divided into a cathodic and an anodic process, which are crucially important to the interpretation of impedance spectra and the understanding of the corrosion mechanism. Because only a trace amount of molecular O_2 dissolves in molten carbonate at 650 °C [25], it will be reduced at first by reacting with molten carbonate to form peroxide, superoxide or bicarbonate ions, which will transport to the solid/molten salt interface to form the corrosion products [26,27]. In the presence of air, the main reduced product of O_2 is peroxide, O_2^{2-}, by the reactions [28,29]:

$$2CO_3^{2-} \rightarrow 2O^{2-} + 2CO_2 \quad (1)$$

$$O_2 + 2CO_3^{2-} \rightarrow 2O_2^{2-} + 2CO_2 \quad (2)$$

After accepting the electrons supplied by the anodic reactions, the peroxide ion will be reduced to O^{2-}, which will in the end combine with metallic ion to form oxides. Therefore the cathodic reaction is

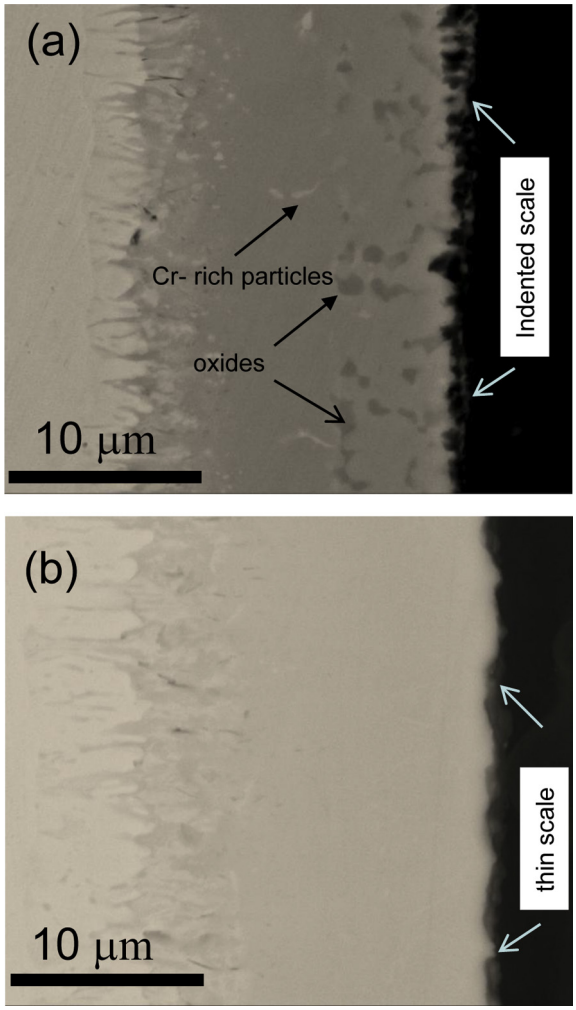

Fig. 5. SEM of the as-deposited coating (a) and as-annealed coating (b) after immersion in molten carbonate for 120 h.

$$O_2^{2-} + 2e^- \rightarrow 2O^{2-} \quad (3)$$

And the anodic reactions are

$$Al \rightarrow Al^{3+} + 3e^- \quad (4)$$

$$Fe \rightarrow Fe^{3+} + 3e^- \quad (5)$$

It can be seen that the corrosion of Al-coated sample with and without high-temperature annealing forms lithium aluminate $LiAlO_2$, a result of the well-known lithiation process of Al_2O_3 [9,12].

When the as-deposited coating is put into the molten salt, it will corrode very fast because of the porous surface that allows easy infiltration of molten salt and large reaction area. The change from the wavy aluminium to a fairly flat surface would indicate a dramatic rearrangement of surface layer during immersion times of the as-deposited coating. Some oxide particles can also be found in the cross-sectional image of the corroded sample of the as-deposited coating in Fig. 5(a), as an evidence of this rearrangement. This process might finish in the first 12 h and is indicated by the slight change in the modulus of impedance afterwards. Although an oxide layer may form on the surface, the morphology of the Al layer is changing, causing the newly formed brittle alumina to peel off. The rugged surface of aluminide surface is also easily subjected to active-passive electrochemical cells [7]. The aluminide formed subsequently has a rough and non-protective scale on its surface and the sample will suffer from active corrosion, so the diffusion of oxide ion species is the rate-limiting step. Jun [9] maintained that the Al–Fe coating with an uneven scale morphology may suffer from localized attack on the coating surface and the growth of corrosion products inside the coating layer. Such corrosion behaviour at the surface was thought to be associated with rough surface texture, inhomogeneous composition distribution, and microstructural defects. Considering the porous scale on the surface and the long line at the low-frequency part of the impedance map, the model in Fig. 7(a) is proposed to explain the impedance data [30]. R_e, R_a and R_c are electrolyte, cathodic and anodic charge-transfer resistance, respectively. A Constant Phase Element (CPE) Q_{dl}, is used to replace the double-layer capacitance, C_{dl}, in the simulation process, for dispersion effect is very common in corrosion of molten salt; Y_{dl} is the numerical value of the admittance of Q_{dl} and n_{dl} the dispersant coefficient. Z_d is the diffusion-related impedance, whose value is:

$$Z_d = A_d(j\omega)^{nd} \quad (6)$$

where A_d is the modulus of Z_d, associated with the solubility and diffusion coefficient of oxidants in the melt, and n_d ($-1 < n_d < 0$), the coefficient of Z_d. When $n_d \geq -0.5$, the diffusion is infinite-length-diffusion and Z_d becomes Warburg impedance, Z_W; when $n_d > -0.5$, Z_W is influenced by tangential diffusion; when $n_d < -0.5$, the diffusion path was blocked to some extent. As can be seen from the simulated data in Table 2, the diffusion impedance is classified as Warburg impedance only for the data of 2 h, indicating the effect of oxide on the diffusion of ionic species of oxygen can be neglected at 2 h; the oxides formed on the surface have a great effect on the diffusion process after 12 h. Frangini and Loreti [31] ascribed this infinite diffusion to the insufficient barrier properties of the scale because of lithiation process when studying the corrosion of 310s stainless steel in molten carbonate in the temperature range between 575 and 695 °C. The diffusion process becomes increasingly difficult since A_w increases persistently in the first 72 h though it dips a bit at 120 h. The charge transfer resistance, R_{ct}, reaches its peak at 12 h, when the transfer of the charged particles on the interface is blocked most severely by the outgrowth of oxides. The drop of R_{ct} after 12 h can be attributed to the brittleness of alumina or lithium aluminate which cracks and peels off when getting thick [12] or the formation of more porous oxide during the lithiation process [32]. At 12 h, the Y_{dl} value reaches the minimum but with the largest value of n_{dl}, and R_{ct}, indicating that an oxide layer with a smoother surface and smaller porosity, compared with other time, possibly appears on the sample at this time.

Fe – 40 at. % Al – 0.5 at. %B, Cu – 30 at.% Al and Ni_3Al alloy forming a protective oxide layer after an extended immersion in molten $(0.62Li + 0.38K)_2CO_3$ at 650 °C were reported, and the two capacitance loops of the impedance map were attributed to the capacitance of the oxide layer in low-frequency part in series with that of the double layer at the melt/scale interface in low-frequency part [30,33,34], as shown in the proposed model in Fig. 7(b). The high polarization resistance (250 Ω cm^2) at 2-h of immersion indicates a protective scale is on the surface of the as-annealed sample, in comparison with that of as-deposited coating (90 Ω cm^2). The R_f and C_f corresponding to the low-frequency loop are the resistance and the capacitance of the oxide film, respectively. This model can be used to explain the corrosion mechanism of the as-annealed sample because similar impedance spectra and a protective scale are found. The parameters of the simulated data are listed in Table 3, where a CPE, Q_f, is used to replace C_f considering the dispersant effect, and represented by Y_f and n_f. The corrosion

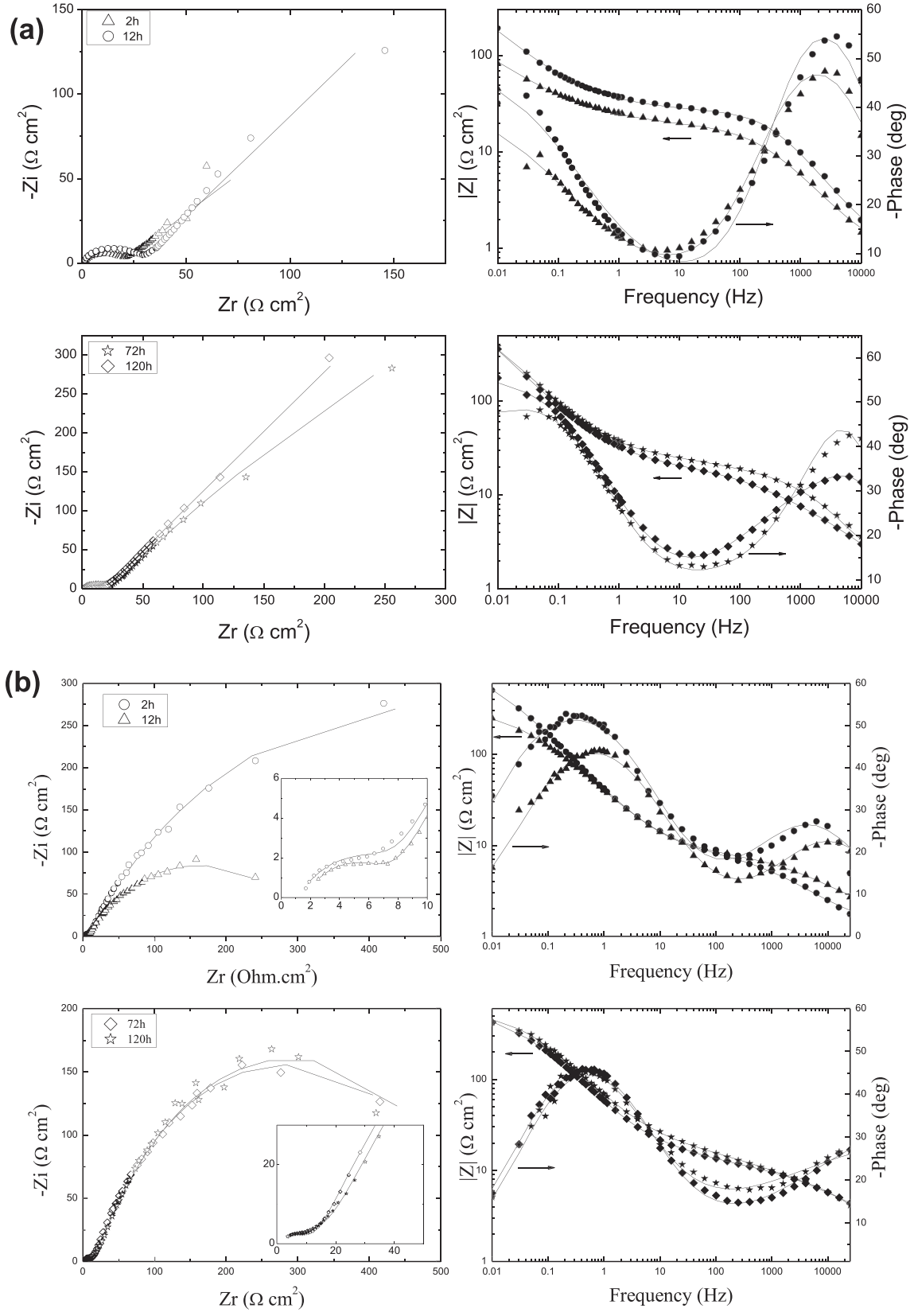

Fig. 6. Nyquist (open marks) and Bode (closed marks) plots for the corrosion process of as-deposited coating (a) and as-annealed coating (b) at different immersion time. Scattered points are measured data and lines are simulated data. The inserts in (b) serve to magnify the high-frequency loops.

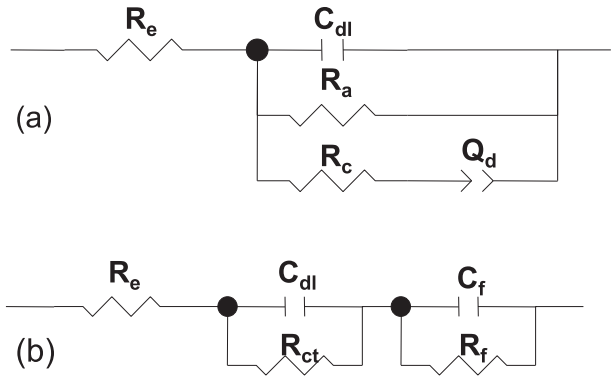

Fig. 7. Equivalent circuits for simulating the impedance data of as-deposited coating (a) and as-annealed coating (b).

process is controlled by the transport of the charged particles moving through the dense scale since R_f is much larger than R_{ct}. The increase of R_{ct} suggests that the transfer of charged ions on the scale/melt interface is becoming more difficult along the growth of oxide layer. However, there is a significant drop of R_f from 941.8 to 310.7 Ω cm^2 between 2 h and 12 h, and this can be attributed to the lithiation of Al_2O_3, a process happening after the formation of oxide [32] and producing more conductive α-$LiAlO_2$ [12]. The corrosion rate of the alloys is proportional inversely to the value of the polarization resistance, R_{pol}, which can be approximated by the subtracting the high-frequency impedance at 10 kHz from the low frequency at 10 mHz. The high R_{pol} value at 2 h for the as-annealed sample (518 Ω cm^2) is as 5.76 times as that of the as-deposited sample (90 Ω cm^2), indicating a slow corrosion process of the as-annealed sample. Since the corrosion process involves the transport of O^{2-} through the scale, the high R_f can be a result of the low O^{2-} conductivity of the scale. From 12 h onward, the increasing charge-transfer resistance, R_{ct}, is a result from the growth of oxide layer. Since the value of parameter Y can be approximately expressed in

$$Y \approx C = \varepsilon_0 K \gamma A/d \tag{7}$$

where ε_0 is the dielectric constant of air, K the relative dielectric constant of the medium, γ the surface porosity, A the effective area of electrode, and d the half-thickness of capacitance. The decrease of Y_f is due the lithiation process, which changes the permittivity, ε_0, of the scale during and the half-thickness of capacitance, d. Y_{dl} value increases continually from 8.77×10^{-4} Ω^{-1} S^{-n} cm^{-2} at 2 h to 2.60×10^{-3} Ω^{-1} S^{-n} cm^{-2} at 120 h, and the reason for this might be the change of the surface condition of the oxide layer; i.e., the oxide layer is getting more porous and its surface is also roughening, a typical process owing to lithiation process [32]. Although taking on a higher porosity and rougher surface, the oxide layer on the high-temperature annealed sample is growing thicker, providing better protection to the substrate materials.

Table 2
Simulated parameters for the EIS of as-deposited Al coating at different immersion time.

Time	R_e Ω cm^2	Y_{dl} Ω^{-1}S^{-n}cm^{-2}	n_{dl} Ω^{-1} S^{-n} cm^{-2}	A_d Ω S^{-n} cm^2	n_d Ω S^{-n} cm^2	[a]R_{ct} Ω cm^2
2 h	0.81	2.53×10^{-4}	0.74	19.23	−0.48	18.01
12 h	1.01	7.05×10^{-5}	0.82	34.97	−0.56	26.02
72 h	0.87	3.48×10^{-4}	0.59	66.93	−0.64	23.64
120 h	1.09	7.94×10^{-4}	0.57	61.77	−0.64	19.57

[a] $R_{ct} = R_a R_c/(R_a + R_c)$.

Table 3
Simulated parameters for the EIS of as-annealed Al coating at different immersion time.

Time	R_e Ω cm^2	Y_{dl} Ω^{-1} S^{-n} cm^{-2}	n_{dl}	R_{ct} Ω cm^2	Y_f Ω^{-1} S^{-n} cm^{-2}	n_f	R_f Ω cm^2
2 h	1.17	8.77×10^{-4}	0.59	6.80	7.69×10^{-3}	0.67	941.8
12 h	1.58	4.51×10^{-4}	0.60	6.03	8.41×10^{-3}	0.63	310.7
72 h	1.51	1.17×10^{-3}	0.42	14.44	5.66×10^{-3}	0.67	540.5
120 h	1.53	2.60×10^{-3}	0.36	20.39	4.83×10^{-3}	0.68	542.5

The as-annealed sample forms a α-$LiAlO_2$ scale without the $LiFeO_2$ layer on the top that is found on the FeAl alloy Fe − 40 at. % Al − 0.5 at. % B under the same condition [7,14]. The reason for this is possibly the active element of Cr in the coating that will enhance the formation of pure alumina scale thanks to the Third Element Effect (TEE) [35]. The scale on the as-deposited coating suffered from persistent active corrosion even though a continuous layer of Al–Fe layer was formed on the surface after 120-h immersion at 650 °C. The corrosion process is a combination of the diffusion of oxygen ion and lithium ion into the initially produced crack as a result of the surface rearrangement in the initial stage. The localised formation of oxides plus lithiation process will crack the scale, causing new active points, which are possibly to cause another run of localised corrosion. On the other hand, the lithiation process shows an insignificant effect on the corrosion of the as-annealed coating, and its effect confines only to the initial stage, and the transport of charged particles in the scale is the rate-limiting step.

4. Conclusion

Electrochemical impedance is used to study the corrosion behaviour of Al coated sample without high-temperature annealing at 850 °C. The as-annealed coating shows better corrosion resistance compared with the Al–Fe intermetallics coating formed in-situ on as-deposited coating during the corrosion process, even though the latter shows higher aluminium content on the surface. The microstructure of the coating is proposed to be crucially important for the corrosion resistance of the aluminide, because pores and crack is going to let through the oxygen ion species or lithium ion to create the active area inhibiting the formation of a protective scale.

Acknowledgements

This work was supported by the National Natural Science Foundation of China under contract No. 51371183 and 50971129. The authors are grateful to Dr J. Ma from the State Key Lab for Corrosion and Protection, Institute of Metal Research, Chinese Academy of Science, for the preparation of Al coating by AIP and the assistance in preparing the manuscript.

References

[1] M. Spiegel, P. Biedenkopf, H.J. Grabke, Corros. Sci. 39 (1997) 1193–1210.
[2] B. Zhu, G. Lindbergh, A. Simonsson, Corros. Sci. 41 (1999) 1515–1528.
[3] B. Zhu, G. Lindbergh, A. Simonsson, Corros. Sci. 41 (1999) 1497–1513.
[4] S. Frangini, J. Power Sources 182 (2008) 462–468.
[5] R.A. Donado, L.G. Marianowski, H.C. Maru, J.R. Selman, J. Electrochem. Soc. 131 (1984) 2535–2540.
[6] R.A. Donado, L.G. Marianowski, H.C. Maru, J.R. Selman, J. Electrochem. Soc. 131 (1984) 2541–2544.
[7] S. Frangini, Oxid. Met. 53 (2000) 139–156.
[8] C.L. Zeng, W. Wang, W.T. Wu, Oxid. Met. 53 (2000) 289–302.
[9] J.G. Gonzalez-Rodriguez, M. Cuellar-Hernandz, M. Gonzalez-Castaneda, V.M. Salinas-Bravo, J. Porcayo-Calderon, G. Rosas, J. Power Sources 172 (2007) 799–804.
[10] J.H. Jun, J.H. Jun, K.Y. Kim, J. Power Sources 112 (2002) 153–161.

[11] A. Aguero, F.J. Garcia de Blas, M.C. Garcia, R. Muelas, A. Roman, Surf. Coat. Technol. 146–147 (2001) 578–585.
[12] F.J. Pérez, D. Duday, M.P. Hierro, C. Gomez, A. Aguero, M.C. Garcia, R. Muela, A. Sanchez Pascual, L. Martinez, Surf. Coat. Technol. 161 (2002) 293–301.
[13] J.E. Indacochea, I. Bloom, M. Krumpelt, T.G. Benjamin, J. Mater. Res. 13 (1998) 1834–1839.
[14] P.Y. Guo, C.L. Zeng, N. Wang, Y. Shao, J. Power Sources 217 (2012) 485–490.
[15] S. Frangini, A. Masci, Surf. Coat. Technol. 184 (2004) 31–39.
[16] S. Frangini, S. Loreti, A. Masci, J. Fuel Cell Sci. Technol. 2 (2005) 60–64.
[17] US Patent, No. US2002/6372374, http://www.freepatentsonline.com/6372374.html.
[18] C.Y. Yuh, R. Johnsen, M. Farooque, H.C. Maru, J. Power Sources 56 (1995) 1–10.
[19] C.Z. Xu, S.M. Jiang, Z.B. Bao, J. Gong, C. Sun, Corros. Sci. 51 (2009) 1467–1474.
[20] C.L. Zeng, J. Li, Electrochim. Acta 50 (2005) 5533–5538.
[21] Y.W. Cui, R. Kato, T. Omori, I. Ohnuma, K. Oikawa, R. Kainuma, K. Ishida, Scr. Mater. 62 (2010) 171–174.
[22] J.P.T. Vossen, R.C. Makkus, A.H.H. Jansen, J.H.W. de Wit, Mater. Corr. 48 (1997) 228–236.
[23] H. Morita, M. Kawase, Y. Mugikura, K. Asano, J. Power Sources 195 (2010) 6988–6996.
[24] Y. Kawabata, N. Fujimoto, M. Yamamoto, T. Nagoya, M. Nishida, J. Power Sources 86 (2000) 324–328.
[25] R.E. Andersen, J. Electrochem. Soc. 126 (1979) 328–334.
[26] A.J. Appleby, S.B. Nicholson, J. Electrochem. Soc. 127 (1980) 759–760.
[27] G.B. Dunks, D. Stelman, Inorg. Chem. 22 (1983) 2168–2177.
[28] M. Cassir, B. Malinowska, W. Peelen, K. Hemmes, J.H.W. de Wit, J. Electroanal. Chem. 433 (1997) 195–205.
[29] T. Nishina, I. Uchida, J.R. Selman, J. Electrochem. Soc. 141 (1994) 1191–1198.
[30] C.L. Zeng, W. .Wang, W.T. Wu, Corros. Sci. 43 (2001) 787–801.
[31] S. Frangini, S. Loreti, J. Power Sources 160 (2006) 800–804.
[32] C.S. Ni, L.Y. Lu, C.L. Zeng, Y. Niu, Corros. Sci. 53 (2011) 1018–1024.
[33] C.L. Zeng, P.Y. Guo, W.T. Wu, Electrochim. Acta 49 (2004) 1445–1450.
[34] J.G. Gonzalez-Rodriguez, E. .Mejia, M.A. Lucio-Garcia, V.M. Aalinas-Bravo, J. Porcayo-Calderon, A. Martinez-Villafane, Corros. Sci. 51 (2009) 1619–1627.
[35] Y. Niu, S. Wang, F. Gao, Z.G. Zhang, F. Gesmundo, Corros. Sci. 50 (2008) 345–356.